

Cooperative Car-Following Control: Distributed Algorithm and Impact on Moving Jam Features

Meng Wang, Winnie Daamen, Serge P. Hoogendoorn, and Bart van Arem, *Member, IEEE*

Abstract—We design controllers and derive implementable algorithms for autonomous and cooperative car-following control (CFC) systems under a receding horizon control framework. An autonomous CFC system controls vehicle acceleration to optimize its own situation, whereas a cooperative CFC (C-CFC) system coordinates accelerations of cooperative vehicles to optimize the joint situation. To realize simultaneous control of many vehicles in a traffic system, *decentralized* and *distributed* algorithms are implemented in a microscopic traffic simulator for CFC and C-CFC controllers, respectively. The impacts of the proposed controllers on dynamic traffic flow features, particularly on formation and propagation of moving jams, are investigated through a simulation on a two-lane freeway with CFC/C-CFC vehicles randomly distributed. The simulation shows that the proposed decentralized CFC and distributed C-CFC algorithms are implementable in microscopic simulations, and the assessment reveals that CFC and C-CFC systems change moving jam characteristics substantially.

Index Terms—Car-following, cooperative systems, receding horizon control, distributed algorithm, moving jam.

I. INTRODUCTION

ONE of the main achievements in transportation science and technology in the past decades is the emergence of intelligent vehicles. Intelligent vehicle systems support or even take over drivers in performing driving tasks such as car-following or lane-changing and are seen as a promising approach in improving traffic safety, efficiency and sustainability [1]. In general, intelligent vehicle systems can be categorized into two groups, i.e., autonomous systems and cooperative systems. Autonomous vehicles do not communicate with others. They rely solely on their on-board sensors and make control decisions for their own sake [2]–[4]. On the contrary, cooperative or connected vehicles ‘talk’ to each other via Vehicle-to-Vehicle (V2V) and/or Vehicle-to-Infrastructure (V2I) communications to enhance the perception of the driving environment and/or to assist cooperative vehicles in maneuvering together under a common goal [5]–[9].

The Adaptive Cruise Control (ACC) system is the earliest car-following control (CFC) system, which specifically aims

Manuscript received March 11, 2015; revised July 1, 2015 and September 29, 2015; accepted November 25, 2015. This work was supported by Shell under the project *Sustainability Perspectives of Cooperative Systems*. The Associate Editor for this paper was L. Vlacic.

The authors are with the Department of Transport and Planning, Delft University of Technology, Delft 2628, The Netherlands (e-mail: M.Wang@tudelft.nl).

Color versions of one or more of the figures in this paper are available online at <http://ieeexplore.ieee.org>.

Digital Object Identifier 10.1109/TITS.2015.2505674

at enhancing driving comfort [2], [6], [7]. The most widely used ACC controller is a PD controller, where the vehicle acceleration is proportional to the gap and the derivative of the gap (relative speed with respect to the preceding vehicle) at car-following conditions. This type of controller has been extensively studied [2], [6], [10]–[12]. The control strategy is referred to as constant time headway (CTH) policy. Extensions of this ACC controller have been used to design ACC systems with variable time gap policies [13] and cooperative ACC (CACC) systems by including the acceleration of the predecessor [2], [6], [7], [14] and positions and speeds of multiple leaders [15]. However, there is no safety mechanism in this model. Under critical conditions, ACC systems have to be overruled by drivers and hard braking has to be performed to avoid a collision [16]. The operation of the extended CACC controllers requires a high penetration rate of CACC systems, i.e., both the leader and the follower have to be equipped vehicles. The cooperation embedded in this type of CACC systems is based on improving the situation awareness by cooperative sensing [9]. There is no cooperation in the decision-making process.

Car-following models are used as state feedback algorithms for ACC systems. The Optimal Velocity Model (OVM) is used to describe the ACC vehicle behavior [17], [18]. The OVM regulates the speed of the controlled vehicle towards an optimal speed, which is a function of the following gap. Unfortunately, the optimal velocity model is not collision free. The Intelligent Driver Model (IDM) is also used to design ACC controllers, with a driving strategy that varies parameters according to traffic situations to mitigate congestion at bottlenecks [19], [20]. Although benefits on capacity are gained through the IDM controller, physical limits such as minimum allowed deceleration and limited sensor detection range are not explicitly included in the model.

Artificial intelligence (AI) techniques are also used to design ACC systems. A rule-based controller is proposed for generic intelligent driver support systems [21]. The vast number of rules and scenarios involved makes the controller highly non-linear and it is not straightforward to gain insights into the properties of the controller. Other AI technologies are also reported in ACC controller design, such as fuzzy logic or self-learning systems [3], [22], [23].

Model predictive control, also called receding horizon control, is used in the design of ACC and CACC controllers. Compared to other control approaches, model predictive control is a flexible approach in dealing with multiple design criteria and constraints on state and control variables. A linear quadratic regulator (LQR) is used for longitudinal control of automated

vehicles [24], [25]. In this special ACC controller, the reference acceleration can be calculated with a linear feedback control law of the state. Model predictive ACC controllers, where the reference acceleration is assessed in a receding horizon way have been proposed [26], [27]. The ACC controller aims at minimizing deviation from desired gap, deviation from predecessor speed, accelerations and jerk, and the deviation from a human desired acceleration calculated with Helly model [26]. However, the resulting traffic flow stability properties of the controllers are not examined [26], [27].

In our previous work, we proposed a generic receding horizon control approach based on Pontryagin's Principle to design both *autonomous* CFC and *cooperative* CFC (C-CFC) systems [4], [9]. The autonomous and cooperative CFC systems include a complex cost function of non-quadratic form that gives high penalty when the subject vehicle approaches the predecessor at small gaps. This mechanism guarantees that at safety-critical conditions, the controllers take safety as first priority and hence can avoid rear-end collision with the predecessor. Safety performance of the controllers has been verified in [4] and [9]. The approach is flexible in deriving cooperative CFC algorithms that are based on sharing information to improve situation awareness, i.e., cooperative sensing, and on maneuvering together under a common objective, i.e., cooperative control [9]. A centralized communication and optimization scheme is proposed and tested in a platoon of 10 cooperative vehicles [9]. The computational load of the centralized algorithm increases with the number of cooperative vehicles in the platoon due to the expansion of dimensionality of state and control input space and becomes *computationally intractable* when the size of the platoon increases substantially in real traffic systems with high penetration rates of cooperative vehicles. Therefore, it is still challenging to implement receding horizon controllers for autonomous and cooperative vehicle systems in large-scale traffic simulations. Furthermore, systematic investigation of the impacts of autonomous and cooperative vehicles with receding horizon controllers on *macroscopic* traffic flow and sustainability have not been reported due to the lack of efficient algorithms and hence their impacts on traffic flow have not been understood sufficiently.

In this article, we propose efficient algorithms for autonomous and cooperative CFC systems under a receding horizon control framework. An autonomous CFC vehicle optimizes its own situation. When two or more C-CFC vehicles form a platoon, the distributed C-CFC algorithm entails neighboring cooperative vehicles transmit their most recent state information and predicted control information via V2V communication to facilitate the decision-making of neighbors and minimize a joint cost function consisting their own situation and the situation of their follower. Even when one C-CFC vehicle is followed by an uncontrolled vehicle where V2V communication is not feasible, the C-CFC vehicle can still exhibit cooperative behavior by predicting the uncontrolled follower behavior and minimizing the joint cost. To realize simultaneous control of many vehicles in a traffic system, *decentralized* and *distributed* algorithms are proposed and implemented in a microscopic traffic simulator for CFC and C-CFC controllers respectively. The impact of the proposed controllers on traffic

flow dynamics, particularly on formation and propagation of moving jams, is investigated through simulation on a two-lane freeway, with CFC/C-CFC vehicles randomly distributed. The simulated freeway stretch constitutes a traffic system with more than 500 vehicles running in the network.

The main contributions of this article are the fast distributed receding horizon cooperative control algorithm that is scalable to large-scale platoons and the new insights into the collective traffic flow characteristics with CFC and C-CFC vehicles.

The rest of the paper is organized as follows. First, the mathematical formulation of the autonomous CFC controller and the corresponding decentralized implementation algorithm is presented in Section II. Following that, the C-CFC controller is formulated and the distributed algorithm is described. Section IV illustrates the experimental design to test the applicability of the proposed algorithms and to assess the impact of the proposed systems. The simulation results are discussed in Section V.

II. AUTONOMOUS CONTROLLER AND DECENTRALIZED ALGORITHM

CFC systems operate in two modes, being following mode and cruising mode [4]. In cruising mode, the CFC system aims to maximize travel efficiency and comfort, while in following mode the system aims to maximize safety in addition to efficiency and comfort. The two modes are distinguished by a critical gap s_f determined by the controller parameters of free/desired (cruising) speed and the desired gap t_d . Note that CFC vehicles operate *autonomously*, i.e., neighboring CFC vehicles do not communicate with each other, nor do they coordinate their behavior when making their control decisions [4]. It is assumed that the lane-changing decisions of CFC vehicles are made by human drivers and vehicle steering is executed by human drivers.

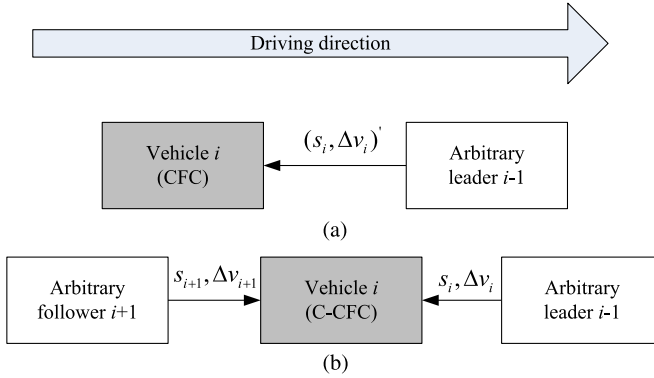
In the remainder of this section, we describe the autonomous CFC controller formulation of CFC systems and present the implementation algorithms in microscopic simulations.

A. Autonomous Controller Formulation

The system state \mathbf{x} from the perspective of a CFC vehicle is defined by the gap (or distance) s_i and relative speed $\Delta v_i = v_{i-1} - v_i$ with respect to the arbitrary leader $i-1$, $\mathbf{x} = (s_i, \Delta v_i)^T$, where v_{i-1} and v_i denote the speed of leader and that of the CFC vehicle respectively, as shown in Fig. 1(a). When following an arbitrary leader, the system state can be estimated with information from in-vehicle sensors, e.g., forward-looking radar. For the sake of control approach illustration, we assume the duality problem of state estimation has been solved elsewhere. Hence, we do not consider noise in the data from the sensors.

Let $\mathbf{u} = u_i$ denote the controlled acceleration of vehicle i . At each sampling time, the receding horizon CFC controller solves a finite horizon optimal control problem at current time t_k with initial state $\mathbf{x}(t_k)$ as follows:

$$\min_{\mathbf{u}} J(\mathbf{x}, \mathbf{u}) = \min_{\mathbf{u}} \int_{t_k}^{t_k + T_P} \mathcal{L}(\mathbf{x}(\tau), \mathbf{u}(\tau)) d\tau \quad (1)$$

Fig. 1. Definition of state variable \mathbf{x} and control variable \mathbf{u} .

subject to the system dynamics equation:

$$\frac{d}{dt}\mathbf{x} = \frac{d}{dt} \begin{pmatrix} s_i \\ \Delta v_i \end{pmatrix} = \begin{pmatrix} \Delta v_i \\ u_{i-1} - u_i \end{pmatrix} = \mathbf{f}(\mathbf{x}, \mathbf{u}) \quad (2)$$

and admissible constraints of control and state [4]:

$$\mathbf{u}(t) \in \mathcal{U} \text{ and } \mathbf{x}(t) \in \mathcal{X}, \quad \forall t \geq 0. \quad (3)$$

In Eq. (1), J denotes the cost functional to be minimized. \mathcal{L} denotes the running cost and T_p denotes the prediction horizon. u_{i-1} denotes the acceleration of the predecessor. For an arbitrary leader, the *constant speed heuristics* is used to predict the behavior of the predecessor in the prediction horizon, i.e., $u_{i-1} = 0$. The feedback nature of the receding horizon process can correct the mismatch between the prediction and the real dynamic behavior of the predecessor [4].

Note that although the linear system model (2) may not adequately describe the vehicle dynamics near physical limits, e.g., tire force saturation due to emergency maneuvers, we are primarily interested in normal vehicle operations in this work where the nonlinear vehicle dynamics can be omitted.

The running cost function is specified as:

$$\mathcal{L} = \begin{cases} \underbrace{\frac{c_1 \Delta v_i^2 \Theta(-\Delta v_i)}{s_i}}_{\text{safety}} + \underbrace{c_2 (s_d - s_i)^2}_{\text{efficiency}} + \underbrace{\frac{u_i^2}{2}}_{\text{comfort}}, & \text{if } s_i \leq s_f \\ \underbrace{c_3 (v_0 - v_i)^2}_{\text{efficiency}} + \underbrace{\frac{1}{2} u_i^2}_{\text{comfort}}, & \text{if } s_i > s_f. \end{cases} \quad (4)$$

s_f is the gap threshold distinguishing cruising mode ($s_i > s_f$) from following mode ($s_i \leq s_f$). The gap threshold is determined by a user-defined desired time gap t_d at following mode, the desired speed v_0 , and the minimum gap between vehicles at standstill conditions s_0 :

$$s_f = v_0 t_d + s_0. \quad (5)$$

Θ is the Heaviside function [4], ensuring that the safety cost only occurs when approaching the preceding vehicle. s_d is the desired gap, which is determined by the current speed and a desired time gap t_d :

$$s_d = v_i(t) t_d + s_0. \quad (6)$$

The gap policy of (6) follows the *constant time gap* policy [2]. The framework allows implementation of variable time gap policies [4]. The running cost formulation (4) is refined based on the ACC controller in [4], and allows smoother transition between cruising mode and following mode.

The running cost function (4) contains multiple criteria of safety, efficiency and comfort. Applying Pontryagin's Principle can express the optimal acceleration as the marginal cost of the relative speed [4]. An efficient numerical scheme based on Pontryagin's Principle is used to solve the optimal control problem [28]. For details on the performance and tuning of the controller, we refer to [4], [29].

B. Decentralized Algorithm

When simulating a large scale system with many CFC vehicles as subsystems, the dynamics of neighboring subsystems are decoupled, but the cost function (4) includes coupling terms of neighboring vehicles in the form of relative position and speed with respect to the preceding vehicle. This feature allows straightforward *decentralized* implementation of the CFC control algorithm in microscopic simulation models. At each time instant t_k , each subsystem/vehicle i solves its *local autonomous* optimal control problem of Eqs. (1) and (4), *synchronously*, subject to system dynamics equation (2), state and control constraints (3), and initial conditions. The behavior of its predecessor is predicted using the *constant speed heuristics*, assuming that the predecessor maintain the current speed in the prediction horizon, i.e., $u_{i-1,[t_k, t_k+T_p]} = 0$. The iterative numerical solution algorithm based on Pontryagin's Minimum Principle (iPMP) [28] is used to compute the optimal control/acceleration trajectory $\mathbf{u}_{i,[t_k, t_k+T_p]}$. Only the first sample of the acceleration trajectory $\mathbf{u}_{i,[t_k, t_{k+1}]}$ is implemented to update the system state. The optimal accelerations are re-calculated after each control cycle in a receding horizon manner, using newest information regarding the system state available from on-board sensors.

III. COOPERATIVE CONTROLLER AND DISTRIBUTED ALGORITHM

Cooperative CFC (C-CFC) controllers have been designed in [9] and a *centralized optimization* scheme is implemented for platoon control. Although it shows promising results in controlling platoons with 10 controlled followers, the centralized communication and control is practically unfeasible due to computation and communication requirements [30], [31]. This section synthesizes the cooperative controllers in [9] to a more general formulation and proposes a more efficient distributed algorithm for cooperative platoon.

A. Cooperative Controller Formulation

The C-CFC controller considered here is assumed to be equipped with both a *forward-looking* sensor detecting the gap and relative speed with respect to its predecessor and a *backward-looking* sensor detecting the gap and relative speed of its follower, as depicted in Fig. 1(b). Furthermore, each C-CFC vehicle is equipped with a V2V communication unit

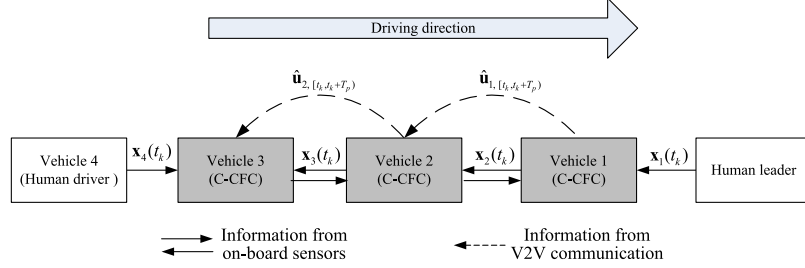


Fig. 2. Distributed communication and control scheme in a cooperative platoon.

to receive the state and control information from the downstream neighboring C-CFC vehicle (when applicable) and to transmit its own state and control information to the upstream neighboring C-CFC vehicle (when applicable), as shown in Fig. 2. The V2V communication is assumed to be perfect and the communication delay is negligible compared to the control cycle of C-CFC controllers. Similar to the design of CFC systems, lane change decisions of C-CFC vehicles are made and lane change maneuvers are executed by human drivers through steering wheels.

To determine the optimal behavior, a C-CFC vehicle predicts the behavior of its predecessor and its follower, based on the information from on-board sensors when direct neighbors are human-driven vehicles and from V2V communication when one or two of its direct neighbors are C-CFC vehicles. The cooperative controller determines its acceleration to minimize its own cost depending on the situation in front as well as the cost of its follower $i + 1$ depending on the situation behind.

To formulate the cooperative controller, we define the system state from the C-CFC vehicle as: $\mathbf{x} = (s_i, \Delta v_i, s_{i+1}, \Delta v_{i+1})^T$. The system dynamics equation is as follows:

$$\frac{d}{dt}\mathbf{x} = \begin{pmatrix} \Delta v_i \\ u_{i-1} - u_i \\ \Delta v_{i+1} \\ u_i - u_{i+1} \end{pmatrix} = \mathbf{f}(\mathbf{x}, \mathbf{u}) \quad (7)$$

where $\mathbf{u} = (u_i)^T$ is the controlled acceleration. u_{i-1} and u_{i+1} denote the acceleration of the leader and follower of vehicle i respectively.

To represent the situations in front and behind the controlled vehicle i , a joint cost function needs to be specified. The most straightforward formulation of the joint cost function is simply the sum of the cost of the two vehicles, which gives the running cost function as:

$$\mathcal{L} = \sum_{n=i}^{i+1} \left\{ \underbrace{\frac{c_1}{s_n} \Delta v_n^2 \cdot \Theta(-\Delta v_n)}_{\text{safety}} + \underbrace{c_2 (s_{d,n} - s_n)^2}_{\text{efficiency}} + \underbrace{\frac{1}{2} u_n^2}_{\text{comfort}} \right\}. \quad (8)$$

Equation (8) shows that the cooperative controller aims to minimize the joint safety, efficiency and comfort cost for itself and its follower. The cooperation only occurs in following mode. In cruising mode, the C-CFC controller functions as the CFC controller in the cruising mode.

The derivation of the optimal acceleration for the C-CFC controller is similar to the CFC controller using Pontryagin's Principle. Its optimal acceleration is determined by the marginal cost of its own relative speed and the marginal cost of its follower's relative speed [9]. The numerical scheme proposed in [28] can solve the cooperative control problem efficiently.

Note that the cooperative vehicle assumes that its follower is minimizing some cost function. While this is the case when vehicle $i + 1$ is a controlled vehicle as vehicle i , it may deviate from the actual behavior of a human-driven vehicle. In this case, a mismatch between the predicted behavior and the actual behavior of vehicle $i + 1$ prevails. Due to the feedback nature of the receding horizon framework and the human-like behavior of controlled vehicle [32], the controller functions well irrespective of the actual behavior specification of the follower $i + 1$ [29]. String stability criterion for C-CFC systems has been derived analytically in [29, Chapter 5] and simulation experiments in [9] have demonstrated string stability of the C-CFC systems.

B. Distributed Algorithm

When controlling a large scale system with many C-CFC vehicles, it is *practically unfeasible* to use a *centralized* implementation of the cooperative algorithm minimizing the performance of the whole system due to the computation and communication requirements [30], [31]. Therefore, the C-CFC algorithm is implemented in a *distributed* fashion, where each vehicle as a subsystem solves a *local cooperative* optimal control problem *synchronously*, taking into account the dynamics of its direct predecessor and follower.

C-CFC vehicle i implements the algorithm as follows:

- 1) Before optimization starts at each time instant t_k , a C-CFC vehicle i receives gap and relative speed with respect to the leader, $s_i(t_k)$ and $\Delta v_i(t_k)$, from its forward-looking sensor. It also receives gap and relative speed with respect to the follower, $s_{i+1}(t_k)$ and $\Delta v_{i+1}(t_k)$, from its backward-looking sensor. If the predecessor is a cooperative vehicle, vehicle i receives predicted control/acceleration trajectory of the predecessor $\hat{\mathbf{u}}_{i-1,[t_{k-1}, t_{k-1}+T_P)}$ obtained from the last time instant t_{k-1} via V2V communication. Vehicle i uses the predicted acceleration trajectory of vehicle $i - 1$ starting from the previous time step t_{k-1} as its assumed

acceleration trajectory starting from current time t_k for predecessor $i - 1$:

$$\hat{\mathbf{u}}_{i-1,[t_k, t_k+T_p]} = \mathbf{u}_{i-1,[t_{k-1}, t_{k-1}+T_p]}. \quad (9)$$

Likewise, vehicle i transmits its predicted control trajectory $\mathbf{u}_{i,[t_{k-1}, t_{k-1}+T_p]}$ obtained from the last time instant t_{k-1} if its follower $i + 1$ is a cooperative vehicle before optimization starts to facilitate the decision-making of vehicle $i + 1$.

- 2) If vehicle $i - 1$ is a C-CFC vehicle, vehicle i predicts the speeds and positions of vehicle $i - 1$ with the assumed acceleration trajectory (9) and initial conditions of $\mathbf{x}_{i-1}(t_k)$. If vehicle $i - 1$ is a human-driven vehicle, vehicle i predicts the speeds and positions of vehicle $i - 1$ with *constant speed heuristics*, i.e., $u_{i-1,[t_k, t_k+T_p]} = 0$.
- 3) Each C-CFC vehicle i solves its *local cooperative* optimal control problem of Eqs. (1), (7), and (8) subject to constraints (3) using the efficient solution algorithm in [4], and determines its own optimal trajectory $\mathbf{u}_{i,[t_k, t_k+T_p]}$.
- 4) The optimal acceleration of each vehicle $\mathbf{u}_{i,[t_k, t_k+T_p]}$ is discretized and the first sample is implemented to update speeds and positions.
- 5) The aforementioned procedure repeats at discrete time instant t_{k+1} , whereas the cooperative vehicles update the assumed control trajectory with:

$$\begin{aligned} \hat{\mathbf{u}}_{i-1,[t_{k+1}, t_{k+1}+T_p]} &= \mathbf{u}_{i-1,[t_k, t_k+T_p]} \\ \hat{\mathbf{u}}_{i,[t_{k+1}, t_{k+1}+T_p]} &= \mathbf{u}_{i,[t_k, t_k+T_p]}. \end{aligned} \quad (10)$$

Note that in this way, the optimization and communication are limited to vehicles *directly* following each other [30], [31], [33], as depicted in a specific platoon formation in Fig. 2.

For cooperative vehicles in microscopic simulations, the accelerations are computed by the iPMP algorithm in a receding horizon way and a communication channel needs to be modeled through which the current gap, relative speed and the predicted acceleration trajectory are transmitted to their cooperative peers. For the sake of evaluation the feasibility and performance of the proposed algorithm, we assume the sensors and V2V communication are perfect.

Here we complete the description on implementation of the algorithms for CFC and C-CFC controllers in traffic simulator. In the sequel, we will present the simulation experimental set-up for assessing the impact of CFC and C-CFC controllers on traffic flow characteristics near a bottleneck, followed by discussions on simulation results. Since our focus of the simulation experiments is on the macroscopic traffic flow impact of autonomous and cooperative vehicles at normal operating conditions, performance verification of the CFC and C-CFC systems at emergency situations are beyond the scope of this study.

IV. ASSESSMENT METHODS AND EXPERIMENTAL SETUP

To test the workings of the proposed algorithms in a dynamic environment and investigate their impacts on traffic flow characteristics, the algorithms are implemented in a microscopic traffic simulator. Extensive traffic simulation experiments are

carried out to evaluate the impact of the proposed algorithms on collective traffic dynamics under a bottleneck, with a focus on the formulation and propagation of moving jams.

A. Bottleneck and Necessary Modeling Aspects

In real traffic, jams are caused by bottlenecks [20]. A *bottleneck* is defined as a local reduction of the road capacity [20], which can be permanent or temporary. Permanent bottlenecks are usually caused by heterogeneity in road infrastructure, such as on-ramps and off-ramps, weaving areas, curves, and uphill and downhill gradients. Temporary bottlenecks are usually caused by accidents, roadworks or temporary change in traffic regulations such as speed limits. We choose the second type of bottleneck induced by temporal changes of speed limits in this study, since the focus of the study is on longitudinal driving control and the car-following maneuvers determines the traffic flow dynamics at this type of bottleneck to a great deal.

When a bottleneck is activated, traffic breaks down at the bottleneck and congested traffic forms upstream of the bottleneck. Different jam patterns at freeway bottlenecks have been reported and defined in literature [20], which can be in general categorized into two types: one with an upstream moving downstream front (jam head) and upstream front (jam tail), which is often called *stop-and-go wave* or *moving jam*, and one with a fixed downstream front at the bottleneck location [20]. The first type of jam is the focus of this study, since it is highly related to decelerating and accelerating behaviors of vehicles.

The jam head of a stop-and-go wave propagates against the driving direction with a *characteristic velocity* in the order of -10 to -20 km/h, while the propagation velocity of the jam tail depends on the traffic states upstream of and in the jam [20], [34]–[37]. One important feature of traffic flow operations at bottlenecks is the so-called *capacity drop* phenomenon. The *capacity drop* refers to the phenomenon that the maximum outflow observed downstream of a jam (referred to as queue discharge flow) is usually smaller than the maximum flow observed before traffic breaks down to congestion (referred to as free flow capacity) [20], [35], [38]. The discrepancy is reported to be around 10–30% [35], [38]. Although the discussions on the capacity drop phenomenon have last for decades [36], [39]–[41], one plausible microscopic explanation for the capacity drop is that drivers tend to keep a larger gap in the transition from an equilibrium state with low speeds to an equilibrium state with high speeds and keep a smaller gap vice versa, i.e., the microscopic hysteresis [42], [43].

The aforementioned traffic flow properties, in particular the backward propagating moving jam and capacity drop phenomena, should be resembled by the traffic simulation model. Furthermore, multiple driver-vehicle classes, e.g., human drivers, CFC and C-CFC systems, should be distinguished in the model. In the following, we describe the chosen simulation model that is able to address these modeling issues.

B. Simulation Model and Network Settings

We choose a simulation model called MOTUS for the impact study. MOTUS is an open-source microscopic traffic simulation

TABLE I
EXPERIMENTAL SCENARIOS FOR IMPACT
STUDY OF CFC/C-CFC SYSTEMS

Scenarios	Traffic composition	Desired time gap (s)
1	100% human drivers	1.3
2	5% CFC + 95% human drivers	1.3
3	10% CFC + 90% human drivers	1.3
4	50% CFC + 50% human drivers	1.3
5	100% CFC	1.3
6	5% C-CFC + 95% human drivers	1.3
7	10% C-CFC + 90% human drivers	1.3
8	50% C-CFC + 50% human drivers	1.3
9	100% C-CFC	1.3

package that is developed in Java [44]. Among many other features, the MOTUS model uses an improved Intelligent Driver Model (IDM) as the car-following module and a lane change model with relaxation and synchronization [44]. It generates realistic traffic wave patterns and free flow capacity, and resembles better multilane traffic at a macroscopic level regarding the amount of traffic volume per lane, the traffic speeds across lanes and the onset of congestion at bottlenecks. For details of the models, we refer to [44].

In MOTUS, the traffic system is represented by a set of interacting objects, including network, vehicle with a driver and on-board unit, and roadside units. The drivers are represented by the lane-changing model and the car-following model. In implementation, we create separate vehicle and driver classes for CFC vehicles and C-CFC vehicles respectively. The CFC and C-CFC algorithms are implemented in the driver classes, replacing the default car-following model and gives accelerations inputs to the vehicles every simulation time step. We remark that the proposed decentralized CFC and the distributed C-CFC algorithms are not limited to the coupling with MOTUS. They can be implemented in *any* microscopic traffic simulator with open interfaces.

Simulation is set up in analogy to a long freeway stretch where stop-and-go wave is the major type of jams in the Netherlands. The road network is a two-lane freeway of 14 km, with a demand of 1900 veh/h on both lanes. Loop detectors are placed every 250 meters on each lane along the freeway, collecting flow and time mean speed every 30 seconds.

A bottleneck is created by posting low speed limits on Variable Speed Limits (VSL) gantries on parts of the freeway. The speed limits are activated for 2 minutes, with speed values of 80 km/h, 60 km/h and 40 km/h displayed at the location of 11 km, 11.5 km and 12 km respectively.

Parameters for MOTUS are chosen based on the face validation on the resultant capacity drop and moving jam propagation characteristics, as we will show in Section V-A.

C. Experimental Scenarios

The variables to be tested for the impact study are the controller type (CFC or C-CFC) and the penetration rate of controlled vehicles in traffic (5%, 10%, 50%, 100%). Together with the reference scenario with 100% human drivers, this amounts to 9 simulation scenarios as shown in Table I. 10 simulation runs are conducted for each scenario.

As discussed in [29], the desired time gap settings for CFC and C-CFC systems impact the road capacity and traffic flow stability. In this study, we choose the same desired time setting as human drivers in MOTUS with $t_d = 1.3$ s. This leads to the same equilibrium flow-density relation and theoretical capacity at the macroscopic level. Hence, the potential changes in dynamic traffic operations depend predominantly on differences of the accelerating and decelerating characteristics of CFC/C-CFC vehicles compared to human-driven vehicles. This allows us to investigate the potentials of advanced model predictive control strategies of CFC/C-CFC vehicles in improving traffic operations without setting smaller time gaps.

D. Assessment Indicators

For each simulation run, the following indicators are calculated:

- Total time spent (TTS) in network. TTS is calculated from the vehicle trajectories of the simulation as:

$$TTS = \sum_{n=1}^{N_{\text{veh}}} ts_n \quad (11)$$

where ts_n denotes the time spent in the network for vehicle n and N_{veh} denotes the total number of vehicles generated in the network during the simulation period.

- Average outflow: Q_{out} . This is measured by the most downstream detector on the freeway stretch and averaged in the simulation period. For homogeneous freeway stretch, this gives an indication on the effective capacity at the bottleneck.

- Jam area: A_{jam} . Jam area is calculated with

$$A_{\text{jam}} = \sum_{i=1}^{K_{\text{sim}}} L_{\text{jam},i} \cdot dT \quad (12)$$

where dT is the detector aggregation time, which is 30 s in this case and K_{sim} is the number of aggregation time intervals for the whole simulation period. $L_{\text{jam},i}$ is the spatial length of the jam at aggregation interval i , and the location of a jam is present is detected by:

$$V_{i,j} \leq V_{\max} \quad (13)$$

where $V_{i,j}$ is the detector speed at time interval i and location $j \cdot dX$. dX denotes the distance between loop detectors, which is 250 meters in this case. V_{\max} is the speed threshold to distinguish free flow and congested traffic, which is 50 km/h. Note that when there is no jam in the network, $A_{\text{jam}} = 0$.

- Flow Q_{jam} and speed V_{jam} of jam area. These are the average flow and speed of the spatio-temporal jam area determined by the speed threshold V_{\max} , which indicate the traffic state in the jam.
- Downstream jam front velocity C_{head} . This is measured with the position of jam head determined by V_{\max} , which reflects how fast the resultant travels. To avoid large estimation errors due to small jam size, we only calculate C_{head} for jams that last longer than 5 minutes.

TABLE II
INDICATORS FOR DIFFERENT SCENARIOS AVERAGED OVER TEN SIMULATION RUNS FOR EACH SCENARIO

Scenarios	TTS (veh·h)	Q_{out} (veh/h)	A_{jam} (km·min)	Q_{jam} (veh/h)	V_{jam} (km/h)	C_{head} (km/h)	DV_{lane} (km/h)	AFC (l/100/km)
1 (100% Human)	562.8	1647	41.7	402	11.7	-11.8	1.7	4.07
2 (5% CFC)	477.4	1818	24.9	1082	28.5	-13.2	3.0	3.91
3 (10% CFC)	453.8	1885	11.5	1586	38.5	-9.3	3.6	3.81
4 (50% CFC)	454.4	1881	10.9	1629	41.4	-7.7	3.8	3.84
5 (100% CFC)	443.8	1897	5.3	1600	37.1	-7.8	2.3	3.69
6 (5% C-CFC)	476.5	1824	26.5	1150	29.9	-14.3	3.4	3.92
7 (10% C-CFC)	442.3	1896	3.6	1554	41.1	-15.3	3.4	3.67
8 (50% C-CFC)	435.1	1897	2.8	1420	46.4	-31.44*	1.9	3.55
9 (100% C-CFC)	433.8	1898	1.9	1456	45.4	n.a.**	1.5	3.49

*: only two jams longer than 5 minutes are observed out of ten simulation runs; ** no jam longer than 5 minutes is observed.

- Mean absolute speed difference across lanes DV_{lane} for the network. This gives an indication on the inhomogeneity of traffic states across lanes.

For sustainability indicators, we focus on average spatial fuel consumption rate per vehicle (AFC). To this end, a modal fuel consumption model is employed, because it captures the operational characteristics of vehicle engines and uses instantaneous vehicle speed and acceleration to calculate (temporal) fuel consumption rate [45]. All model parameters are available in [45]. Assuming the specific engine type in [45], this model estimates instantaneous fuel consumption rate of vehicle n , Ft_n as a function of vehicle speed v_n and acceleration a_n :

$$Ft_n = \begin{cases} \sum_{j=0}^3 b_j v_n^j + c_1 v_n a_n + c_2 v_n a_n^2, & \text{if } a_n \geq 0 \\ \sum_{j=0}^3 b_j v_n^j + c_1 v_n a_n, & \text{if } a_n < 0 \end{cases} \quad (14)$$

where b_j and c_j are model parameters. For details of the fuel consumption model, we refer to [45]. The AFC is calculated by dividing total fuel consumption with the total distance traveled by all vehicles in the network.

The average values of indicators over all simulation runs are summarized in Table II.

Apart from the indicators, we also visualize the simulation results in different scenarios, including the spatial-temporal contour plots of flow Q and speed V , flow-density scatter plots. The contour plots depicts the spatio-temporal evolution of aggregate traffic flow and speed, which give insights into the jam patterns and traffic flow dynamics. In the flow-density plots, we differentiate the whole freeway into upstream, downstream and jam regions when a jam prevails, which gives insights into the differences in the inflow and outflow of a jam area. Furthermore, to gain insights into the changes at microscopic level, we plot the average gap and speed relationships in different scenarios. Particularly, we distinguish the trajectory data samples into the acceleration state, deceleration state and equilibrium state. The different states for each vehicle n at time t are differentiated with an acceleration threshold of 0.01 m/s^2 in acceleration:

- if $a_n > 0.01$, the vehicle is in acceleration state;
- if $a_n < -0.01$, the vehicle is in deceleration state;
- if $a_n \in [-0.01, 0.01]$, the vehicle is in equilibrium state.

The trajectory data points are aggregated into the same spatial and temporal length of the detectors with different states.

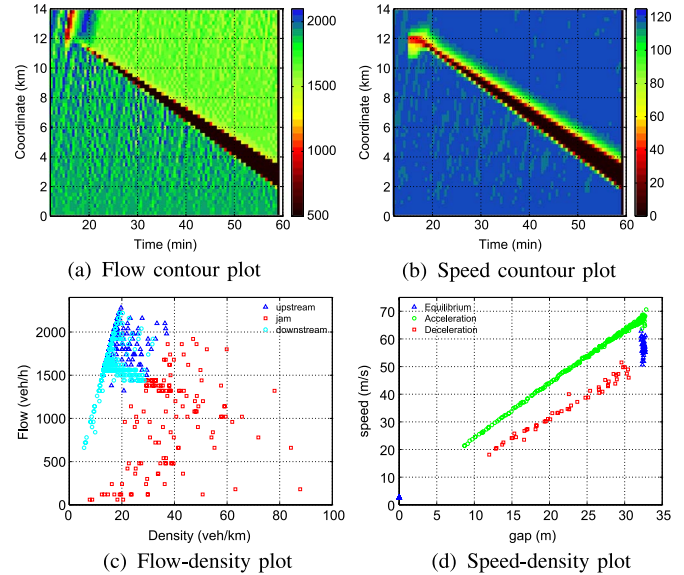


Fig. 3. (a) Flow contour and (b) time mean speed contour plots, and (c) flow-density plots and (d) gap-speed plots in Scenario 1 with 100% human drivers.

V. SIMULATION RESULTS

This section describes the simulation results, with a focus on the impact of CFC and C-CFC systems on formation and propagation of moving jam at the bottleneck. First, the traffic states and jam patterns in the reference case is described, showing the face validity of the simulation model. Then the flow characteristics with CFC and C-CFC systems are discussed subsequently.

A. Verification of the Reference Scenario

In this study, a bottleneck is activated by temporarily changing speed limits on part of the freeway stretch, resulting in a lower road capacity than the demand. Fig. 3(a) and (b) show the spatio-temporal evolution of flow and time mean speed per lane on the simulated freeway collected from loop detectors. As we can see from the figures, the traffic speed drops from 120 km/h to about 40 km/h at around 12 km from 15 minutes, due to the change in speed limits. The speed limits cause vehicles in the bottleneck area to slow down, increasing the density in the bottleneck area and limiting the outflow from the bottleneck. After the vehicles move out of the bottleneck, they start to accelerate back to the free speed, which is around 120 km/h. This leads to a

wave propagating downstream with low flow and high speed in the flow and speed contour plots. The bottleneck is only active for two minutes. Directly after the release of the bottleneck, the desired speeds of vehicles in the bottleneck switch back to 120 km/h. The vehicles in the bottleneck with high density start to accelerate consequently, leading to a high flow and high speed state propagate downstream, as shown in Fig. 3(a) and (b). Traffic flow theorists have shown that the high density state with high flow is not stable [20], [46]. Indeed, after a while, traffic breaks down with speeds degrading gradually, which leads to a persistent moving jam propagating upstream [20], [46].

The average traffic speed and flow in the jam is 11.7 km/h and 402 veh/h respectively, with the jam head, or the downstream jam front, propagating with a characteristic velocity of -11.8 km/h, as shown in Table II. The traffic state downstream of the jam area is quite homogeneous, i.e., there are hardly any variations in the flow and speed, as shown in Fig. 3(a) and (b).

The *capacity drop* phenomenon is clearly visible in the flow contour plot of Fig. 3(a) and the flow-density scatter plot of Fig. 3(c), i.e., outflow from the jam maintain an average value of 1647 veh/h, which is significantly lower than the average inflow of 1900 veh/h. The discrepancy between outflow and the capacity is in accordance with the reported values of around 10–30% [20], [35], [38]. Due to this discrepancy, the size of the jam increases with the course of time, with the upstream jam front (jam tail) traveling upstream with a faster speed than that of the downstream jam front (jam head). This leads to a total jam size of 41.7 veh·h.

It is commonly accepted that the microscopic explanation of the *capacity drop* phenomenon is that drivers keep a larger gap in accelerating phase compared to decelerating phase, i.e., the microscopic hysteresis phenomenon [42], [43]. This common phenomenon is reproduced in our simulation, as depicted by the average gap and speed scatter plots in the decelerating and accelerating phase in Fig. 3(d).

B. Impacts of CFC Systems on Flow Characteristics

Compared to the reference case, scenarios 2–5 with different penetration rates of CFC systems bear some resemblance regarding flow characteristics at the bottleneck. The activation of the bottleneck creates a traffic wave of low flow and high speed traveling downstream, followed by a wave with high flow and high speed propagating downstream immediately after the release of the bottleneck. The bottleneck leads to backward propagating moving jams in all CFC scenarios, as shown with one representative simulation run in Fig. 4.

There are several differences that need special attention when CFC vehicles prevail in the network. We discuss the qualitative differences with Figs. 4 and 5, and the quantitative differences with indicators of Table II. We discuss consecutively traffic efficiency, stability and jam propagation, and sustainability.

1) *Traffic Efficiency*: CFC systems increase traffic efficiency and mitigate the capacity drop phenomenon. The average total time spent (TTS) in the network and jam sizes in scenarios 2–5 are much smaller than in the reference scenario. The TTS and jam size decrease to 477.4 veh · h and 24.9 km · min in scenario 2 from 562.8 veh · h and 41.7 km · min in the reference scenario

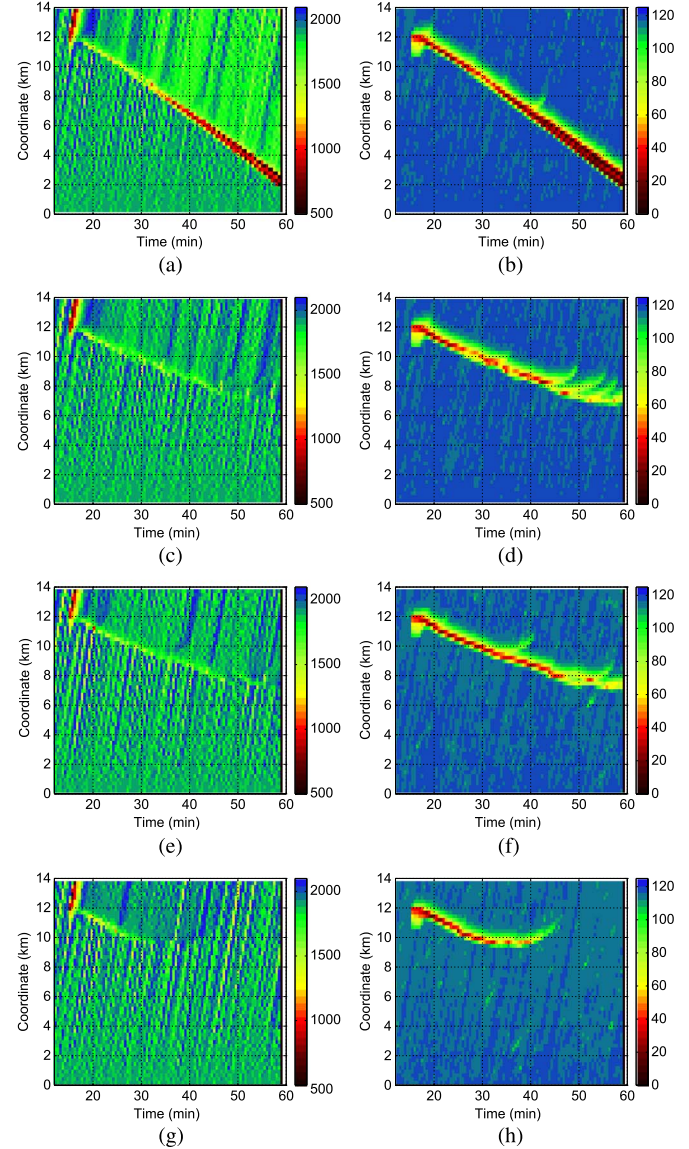


Fig. 4. Spatio-temporal evolution of flow and speed of CFC with different penetration rates (Scenarios 2–5) in one simulation run. (a) Flow of scenario 2 with 5% CFC; (b) speed of scenario 2 with 5% CFC; (c) flow of scenario 3 with 10% CFC; (d) speed of scenario 3 with 10% CFC; (e) flow of scenario 4 with 50% CFC; (f) speed of scenario 4 with 50% CFC; (g) flow of scenario 5 with 100% CFC; (h) speed of scenario 5 with 100% CFC.

respectively. The TTS and jam size decrease further to similar values in scenarios 3 and 4. The TTS and jam size are reduced to only 443.8 veh · h and 5.3 km · min when all vehicles are controlled by the CFC system.

The outflow from jams in scenarios 2 is higher than that of the reference scenario, but still lower than the inflow. Hence the capacity drop and microscopic hysteresis phenomenon remains in scenario 2, as we can see from Fig. 5(a) and (b). As a result, the spatial size of the jam increases with the course of time in scenario 2, as shown in Fig. 4(a) and (b). When the penetration rate increases to 10% and higher, the outflow increases more or less to the value of the inflow, resulting in moving jams with more or less constant sizes, as we can see from Fig. 4(d), (f), and (h). Hence capacity drop is not pronounced in scenarios 3–5, which is also evidenced by the flow-density plots

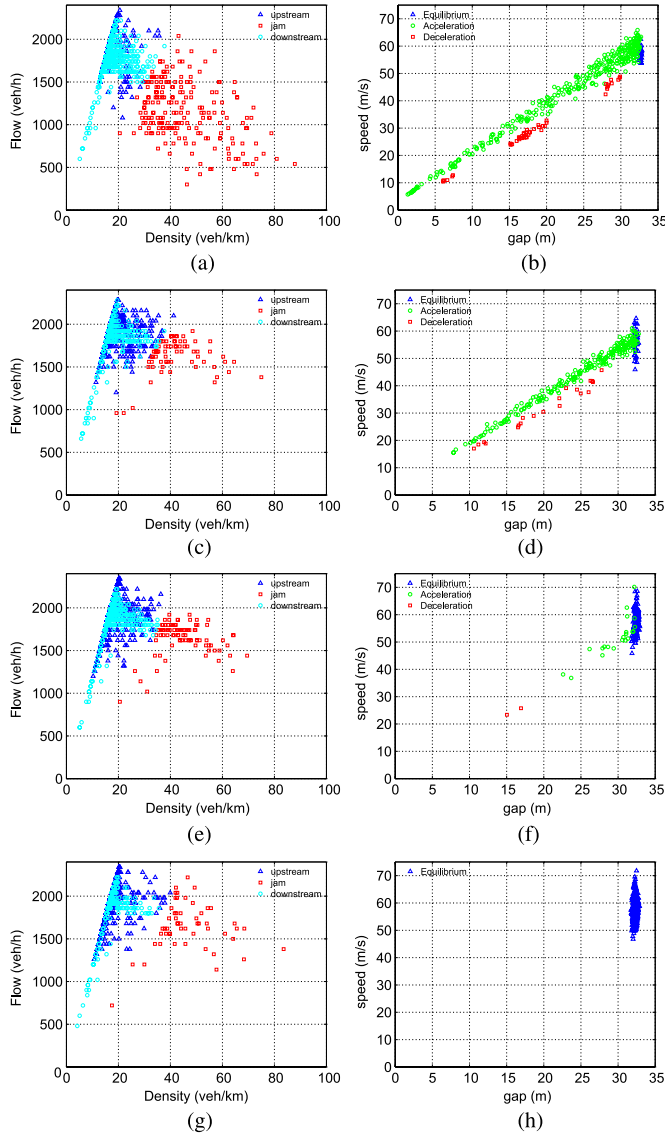


Fig. 5. Flow-density plots for CFC impact study with different penetration rates (Scenarios 2–5) in one simulation run. (a) Scenario 2 with 5% CFC; (b) scenario 2 with 5% CFC; (c) scenario 3 with 10% CFC; (d) scenario 3 with 10% CFC; (e) scenario 4 with 50% CFC; (f) scenario 4 with 50% CFC; (g) scenario 5 with 100% CFC; (h) scenario 5 with 100% CFC.

of Fig. 5(c), (e), and (g) and gap-speed plots of Fig. 5(d), (f), and (h). The reason for this is that the formulation and parameter settings for CFC controllers result in a more agile driving style, i.e., the CFC vehicles accelerate faster towards the high speed state than human drivers under same conditions of gaps (s), relative speeds Δv and speeds v , which leads to smaller headway and hence higher flow in the acceleration transition. Furthermore, the human-driven vehicles following CFC vehicles are convicted to the *follow-the-leader* rule in mixed traffic scenarios, and hence are dragged by the CFC vehicles to keep smaller headways than in scenario 1, which consequently increases the outflow from the jam area.

2) *Stability and Jam Propagation:* As we can see from Fig. 4 and Table II, the traffic speed and flow in the jam of scenario 2 are higher than those in scenario 1. This implies that the CFC vehicles improve the traffic flow stability of the

jam area, i.e., the traffic does not break down to a speed as low as the reference case. When the penetration rate increases to 10% or higher, the stabilization effects are more pronounced, as the average speed in the jam area stays around the bottleneck speed of 40 km/h. The stability effects can be explained by the controller design of CFC systems. As we have explained in the previous work [4], in decelerating transitions, the safety cost due to approaching the preceding vehicle dominates the CFC vehicular behavior. Hence CFC vehicles are more sensitive to the relative speed in the decelerating phase, exhibiting a more anticipative driving style which stabilizes traffic flow approaching the jam tail.

Regarding the propagation of the jam head, although the size and period of the jams are different, they all propagate in the upstream direction after the start of the bottleneck. However, unlike the reference case where the jam head propagates upstream with a *constant characteristic velocity*, the jam propagation velocity differs with different penetration rates of equipped vehicles across scenarios, as shown in Fig. 4 and Table II. In scenario 2, the jam head propagates faster than that of scenario 1 while in scenario 3–5, the jam heads propagate slower than in scenario 1. In scenario 5 as shown in Fig. 5(h), the jam wave first propagates upstream from 17 minutes to about 25 minutes, then it gradually changes its velocity and stays at around 9.75 km for 10 minutes and finally propagates in the *reversed* direction. After a few minutes the jam dissolves when propagating in the downstream direction.

It is noteworthy that several waves propagating in the downstream direction from the jam head are observed in speed contour plots in CFC scenarios, e.g., from around 40 minutes in Fig. 4(b), from around 42 minutes onwards in Fig. 4(d), and from around 34 minutes in Fig. 4(f). This is quite different compared to the homogeneous traffic speeds downstream of the jam area in the reference scenario 1, as shown in Fig. 3(b). These waves are not sustained and vanish in the free flow region after propagating downstream for a few minutes. Although these disturbances do not result in persistent waves, it does raise some concerns on the stability property at the downstream area of the jam. Since the CFC vehicles accelerate faster and keep a smaller gap from the jam area to the downstream free flow area compared to human-driven vehicles, the human-driven vehicles in scenario 2 that follow CFC vehicles also accelerate faster and maintain a smaller gap compared to the normal situations in the reference case. Although this increases the outflow from the jam area, it may destabilize traffic flow downstream of the jam area.

The existence of CFC vehicles in the mixed traffic scenarios of 2–4 increase the inhomogeneity of traffic states across lanes. As we can see from Table II, the average speed differences across lanes in the network are higher in scenarios 2–4 than those in scenarios 1 and 5. The inhomogeneity of traffic states across lanes are caused by the intrinsic differences in the car-following rules between human drivers and CFC vehicles.

3) *Sustainability:* From sustainability perspectives, the reduction of the stop-and-go waves has clear benefits in reducing fuel consumption, since the accelerating and decelerating maneuvers and their durations are substantially reduced with the decreasing size of jams. As we can see from Table II, the

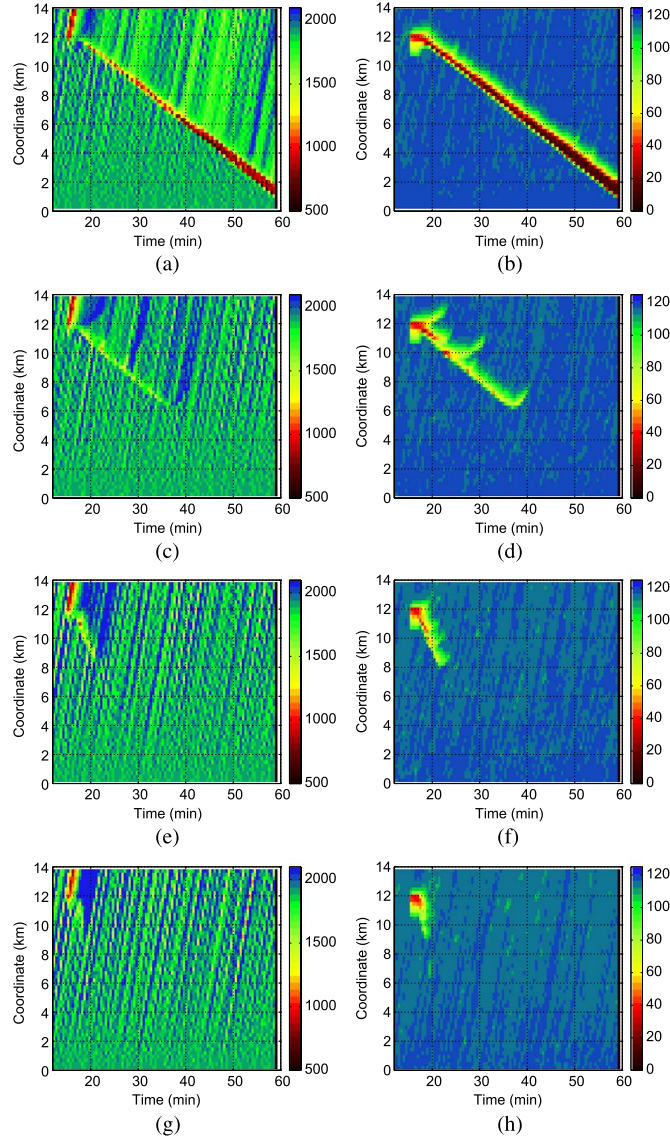


Fig. 6. Spatio-temporal evolution of flow and speed of CCFC with different penetration rates (Scenarios 6–9) in one simulation run. (a) Flow of scenario 6 with 5% CCFC; (b) speed of scenario 6 with 5% CCFC; (c) flow of scenario 7 with 10% CCFC; (d) speed of scenario 7 with 10% CCFC; (e) flow of scenario 8 with 50% CCFC; (f) speed of scenario 8 with 50% CCFC; (g) flow of scenario 9 with 100% CCFC; (h) speed of scenario 9 with 100% CCFC.

average spatial fuel consumption rates are reduced when CFC vehicles are present in the network, and the benefits increase with the increase of penetration rate in general.

C. Impacts of C-CFC Systems on Flow Characteristics

Compared to human drivers and CFC systems, C-CFC systems have clear benefits in improving traffic flow operations and sustainability at the bottleneck type in this study.

1) *Traffic Efficiency*: In scenario 6 with 5% C-CFC vehicles, the average outflow from the jam is 1824 veh/h, which is much higher than 1647 veh/h in the reference case, but still lower than the inflow of 1900 veh/h. Hence the capacity drop phenomenon prevails and spatial jam size increases with the course of time, as shown in Fig. 6(a) and (b). The jam size is in the same order as in scenario 2.

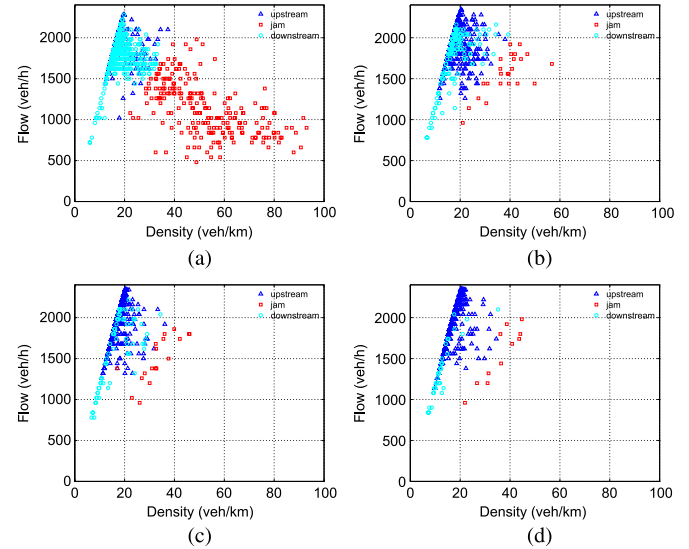


Fig. 7. Flow-density plots for CCFC impact study with different penetration rates (Scenarios 6–8) in one simulation run. (a) Scenario 6 with 5% CFC; (b) scenario 7 with 10% CFC; (c) scenario 8 with 50% CFC; (d) scenario 9 with 100% CFC.

When the penetration rate of C-CFC systems increases to 10% and 50%, the differences between the C-CFC scenarios and their CFC counterparts become apparent. The average outflow is much higher and the TTS and jam size in scenario 7 are much smaller than those in scenarios 6 and 3. The indicators in scenario 7 with 10% C-CFC systems are even better compared scenario 5 with 100% CFC vehicles. As we have shown in previous work [9], C-CFC systems generate more anticipative and responsive accelerating behavior compared to CFC systems, which account for the substantial improvement in traffic efficiency.

In scenarios 8 and 9, after the release of bottleneck, the outflow downstream of the jam area remains at very high values, and the resultant TTS and jam size decrease with the increase of penetration rate of C-CFC vehicles.

The improvement in traffic efficiency with CFC systems are clearly seen in the flow-density plots. As we can see in Fig. 7, the number of data points in the jam area decreases with the increase of C-CFC penetration rate, and the data points are less scattered with the increase of C-CFC penetrate rate.

2) *Stability and Propagation of Jams*: The *cooperative control* strategy of C-CFC systems leads to smoother decelerating behavior and improves stability of flow approaching the jam. As we can see from Table II, the traffic speed and flow in the jam areas are higher than those in the reference scenario 1 and those with their CFC counterparts. In scenarios 7–9, average traffic speeds in the jam are even higher than the bottleneck speed of 40 km/h. This is explained by the controller characteristics, i.e., the smoother behavior of C-CFC controllers decreases the *overshooting* effects in the decelerating transition [9] and vehicles in scenarios 7–9 do not decelerate further to speeds lower than 40 km/h.

Although the bottleneck results in a persistent stop-and-go wave in scenario 6, with only 10% of C-CFC vehicles in the network in scenario 7, the stop-and-go wave dissolves

itself after propagating upstream a few minutes, as we can see from Fig. 6(c) and (d). The stop-and-go waves also dissolve themselves in scenarios 8 and 9, as shown in Fig. 6(e)–(h).

Although the jam head speed still varies across different scenarios with different C-CFC vehicle penetration rates, it is clear that for all scenarios where jams longer than 5 minutes are observed, the jam head in C-CFC scenarios propagates faster compared to the reference case and to their CFC counterparts. The propagation speed also increases with the penetration rate of C-CFC systems. This can be explained by the *distributed cooperative algorithm* that V2V communication enables, i.e., the *current state* and the *predicted acceleration trajectory* of C-CFC vehicles are transmitted to their C-CFC follower when applicable and are taken into account by the C-CFC follower in determining cooperative optimal accelerations. This allows the C-CFC vehicles to react earlier to the downstream disturbances compared to uncontrolled vehicles and CFC vehicles.

Similar to scenarios with CFC systems, we observe several forward propagating waves originating from the jam head characterized with relatively high speeds (between 60 and 80 km/h) and very high flow (around 2000 veh/h), e.g., at about 18 minutes, 24 minutes and 37 minutes in Fig. 6(c) and (d).

Similar to the CFC scenarios, the mixtures of C-CFC and human-driven vehicles in the network increase the inhomogeneity in the traffic states across lanes compared to scenario 1. The average speed difference across lanes is much larger in scenarios 6 and 7 than in scenarios 1, 8, and 9.

3) *Sustainability*: The improvement in sustainability with C-CFC systems is obvious compared to human drivers, as shown in Table II. In all scenarios with C-CFC systems, the average spatial fuel consumption rates are lower compared to the reference scenario 1. Even compared to CFC system, the benefits are still clear. While the average fuel consumption rate in scenario 6 remains at a similar level compared to scenario 2, the average spatial fuel consumption rates with C-CFC systems in scenarios 7–9 are considerably lower than their CFC counterparts in scenarios 3–5, as a result of the reduced jam size. This suggests improvement in sustainability of when C-CFC vehicles travel in networks.

D. Discussion on Changed Flow Characteristics

The impact study reveals some new insights into traffic flow characteristics with CFC and C-CFC systems. In this subsection, we summarize and discuss the changes in flow dynamics at the bottleneck.

1) *Traffic Downstream of Jam Area*: Downstream of the jam area, vehicles are in acceleration transition from low speed state to high speed state. Our simulation shows that under the designed parameter setting, CFC systems lead to more efficient flow moving out of jam and reduce the capacity drop. The microscopic explanation of this change is the responsive behavior of CFC systems, i.e., CFC vehicles recovers the high speed faster than human drivers, and thus they follow with a smaller gap in the accelerating phase. However, this is achieved at the expenses of compromising stability, since *decentralized* CFC vehicles have limited knowledge of their predecessor behavior and make simple assumptions in the state prediction,

i.e., *constant speed heuristics* for predecessors. This has a potential risk for triggering new jams in the downstream area of the jam with CFC systems.

When employing the cooperative control strategy, C-CFC vehicles have better knowledge of the predecessor behavior when they are following their C-CFC peer, and hence can predict the dynamics of the predecessor more accurately. As a result, they are able to react earlier to the accelerating stimuli while at the same time preventing the *overshooting* in the transition from low speed state to high speed state [29]. This leads to smaller headways in the accelerating phase, but also improves traffic stability in the downstream area of a jam.

2) *Traffic Upstream of Jam Area*: Stability/instability of flow approaching the jam tail is an important feature in the formation of jams. The stability is determined by two counteracting processes: the retarded adaptation to the low speed and the ability to anticipate downstream traffic [38]. For the human-driven vehicular flow, the retarded adaptation outweighs the anticipation, and hence the temporary speed drop leads to formation of jam.

The stability of traffic flow approaching the jam tail is improved with CFC vehicles in the network. This is explained by the controller formulation: when CFC vehicles predict costs under decelerating disturbances, the weight on safety cost increases with a decreasing gap in Eq. (4). Hence the CFC vehicles react more to the relative speed with respect to the preceding vehicle. As the relative speed is a simple form of anticipation for the future gap [20], [32], this implies that CFC vehicles exhibits an anticipative driving style in the decelerating phase. Compared to CFC systems, C-CFC systems based on the *cooperative control* strategy lead to more anticipative and smoother decelerating behavior by maneuvering together as a platoon [9], and hence further improve the stability of traffic approaching the jam tail compared to CFC systems.

3) *Propagation of Jam*: For stop-and-go waves in human-driven vehicular flow, the jam head has a characteristic velocity [20]. The jam head velocity changes in scenarios with different penetration rates of CFC systems in traffic. At a low penetration rate of 5%, the jam heads travels faster, while at scenarios with 10% or more CFC vehicles in the network, the jam heads travel slower compared to the reference case. According to kinematic wave theory [34], the jam head velocity is determined by the traffic state in the jam and traffic state downstream of the jam, both influenced by the specific compositions of traffic (penetration rates and locations of CFC vehicles) in the respective areas. This makes the jam head velocity *less characteristic* with CFC/C-CFC systems.

Although the jam head velocity also varies with different penetration rates of C-CFC systems, it is quite clear that the jam head travels much faster when C-CFC systems exist in the network due to V2V communication.

4) *Implications for Dynamic Traffic Management*: The changes in flow characteristics have implications for dynamic traffic management. Under the same strength of a bottleneck, the CFC and C-CFC systems may stabilize the upstream traffic approaching the bottleneck that reduces the probability of traffic break down, which consequently lowers the necessity for the traffic controller to intervene. Even if the jam prevails, the more

efficient outflow due to the presence of CFC/C-CFC systems reduces the size of the jam, which is also favorable for traffic controllers since this implies less control efforts.

However, possible difficulties are expected when controlling traffic flow with CFC/C-CFC systems. Firstly, the resultant jam state is difficult to predict due to the inhomogeneous distribution of controlled vehicles in the network. Furthermore, CFC systems may destabilize traffic flow in the accelerating transition, and hence increase the risk of triggering new jams downstream of the considered jam.

VI. CONCLUSION

In this study, we tested the CFC and C-CFC algorithms in multilane traffic scenarios and examined the impact of CFC and C-CFC systems on traffic flow operations. *Decentralized* algorithms and *distributed* algorithms are proposed and implemented for CFC and C-CFC controllers in the microscopic simulator respectively. The CFC and C-CFC algorithms have been successfully implemented on a large scale system with more than 500 controlled vehicles as subsystems. The proposed algorithms work well under discontinuities in state variables (i.e., gap and relative speed with respect to the preceding vehicle) caused by lane-changing maneuvers and dynamically changing parameters, e.g., free/desired speeds due to variable speed limits. In principle, the decentralized CFC and distributed C-CFC algorithms can be implemented in *any* microscopic simulation model.

Simulation results provide insights into impacts of CFC and C-CFC systems on traffic flow characteristics. CFC systems mitigate the capacity drop phenomenon and improve the stability of traffic flow upstream of the jam area. The jam propagation speed changes with different penetration rates of CFC vehicles in the network, and the jam propagation direction is even reversed in scenarios with high penetration rates, resulting in a new phenomenon which is not observed in human-driven vehicular flow. CFC systems may destabilize traffic downstream of the jam area due to the closer following distance in the transition from low speed state to high speed state. Fuel consumption is reduced with CFC systems in traffic compared to the reference scenario with all human-driven vehicles.

The C-CFC systems employing the cooperative control strategy are more predictive and anticipative, since the predicted acceleration trajectory of the cooperative predecessor is taken into account in the state prediction of the cooperative follower. These characteristics improve the stability at both jam tail and jam head, while at the same time increasing the outflow in the accelerating phase. Under the bottleneck created in this study, the disturbance caused by temporarily reduced speed limits is damped out and hence does not evolve into persistent waves with only 10% C-CFC vehicles in traffic. The fact that C-CFC vehicles predict the future of the predecessor behavior and take into account the expected behavior of the follower has clear benefits in the bottleneck. C-CFC systems stabilize traffic flow and increase the effective capacity of the bottleneck compared to human drivers and CFC systems. One noteworthy flow property is that C-CFC systems result in faster stop-and-go waves propagating upstream due to V2V communications.

At very low penetration rates of CFC and C-CFC vehicles in traffic, e.g., less than 5%, human drivers still dominate the traffic flow characteristics. Hence the flow characteristics remain qualitatively the same, i.e. capacity drop and jam propagation, as the reference case with 100% human drivers.

Note that different types and strengths of bottlenecks may result in jam types and flow patterns other than the stop-and-go waves discussed in this study. Hence, it remains an interesting research question how the proposed decentralized CFC and distributed C-CFC systems influence the characteristics of other jam patterns.

Based on the impact study results, it can be concluded that the CFC and C-CFC system changes flow characteristics substantially, and a roadside controller is likely to be necessary to resolve stop-and-go waves at low penetration rates when human-driven vehicles dominate the flow operations.

Future research is directed to the robust design of the autonomous and cooperative intelligent vehicle controllers in more practical situations where noises and delays prevail in the control loop. Another future research direction is to examine the impact of the proposed systems in active bottlenecks with road geometric inhomogeneities, such as on- and off-ramps. The proposed control algorithms only regulate longitudinal motion of controlled vehicles. Extension of the control algorithms by regulating vehicle steering and orientations in the lateral motion remains an interesting topic in the future [47].

REFERENCES

- [1] P. Varaiya and S. E. Shladover, "Sketch of an IVHS systems architecture," in *Proc. IEEE Veh. Navig. Inf. Syst. Conf.*, 1991, vol. 2, pp. 909–922.
- [2] J. VanderWerf, S. E. Shladover, N. Kourjanskaia, M. Miller, and H. Krishnan, "Modeling effects of driver control assistance systems on traffic," *Transp. Res. Rec.*, vol. 1748, pp. 167–174, 2001.
- [3] G. N. Bifulco, L. Pariota, F. Simonelli, and R. D. Pace, "Development and testing of a fully adaptive cruise control system," *Transp. Res. C, Emerging Technol.*, vol. 29, pp. 156–170, Apr. 2013.
- [4] M. Wang, W. Daamen, S. P. Hoogendoorn, and B. van Arem, "Rolling horizon control framework for driver assistance systems. Part I: Mathematical formulation and non-cooperative systems," *Transp. Res. C, Emerging Technol.*, vol. 40, pp. 271–289, Mar. 2014.
- [5] S. Tsugawa, S. Kato, T. Matsui, H. Naganawa, and H. Fujii, "An architecture for cooperative driving of automated vehicles," in *Proc. IEEE Conf. Intell. Transp. Syst.*, 2000, pp. 422–427.
- [6] B. van Arem, C. J. G. van Driel, and R. Visser, "The impact of cooperative adaptive cruise control on traffic-flow characteristics," *IEEE Trans. Intell. Transp. Syst.*, vol. 7, no. 4, pp. 429–436, Dec. 2006.
- [7] S. E. Shladover, D. Su, and X.-Y. Lu, "Impacts of cooperative adaptive cruise control on freeway traffic flow," *Transp. Res. Rec.*, vol. 2324, pp. 63–70, 2012.
- [8] J. Monteil, R. Billot, J. Sau, and N.-E. El Faouzi, "Linear and weakly nonlinear stability analyses of cooperative car-following models," *IEEE Trans. Intell. Transp. Syst.*, vol. 15, no. 5, pp. 2001–2013, Oct. 2014.
- [9] M. Wang, W. Daamen, S. P. Hoogendoorn, and B. van Arem, "Rolling horizon control framework for driver assistance systems. Part II: Cooperative sensing and cooperative control," *Transp. Res. C, Emerging Technol.*, vol. 40, pp. 290–311, Mar. 2014.
- [10] P. A. Ioannou and C. C. Chien, "Autonomous intelligent cruise control," *IEEE Trans. Veh. Technol.*, vol. 42, no. 4, pp. 657–672, Nov. 1993.
- [11] S. Darbha and K. R. Rajagopal, "Intelligent cruise control systems and traffic flow stability," *Transp. Res. C, Emerging Technol.*, vol. 7, no. 6, pp. 329–352, Dec. 1999.
- [12] R. Rajamani and S. E. Shladover, "An experimental comparative study of autonomous and co-operative vehicle-follower control systems," *Transp. Res. C, Emerging Technol.*, vol. 9, no. 1, pp. 15–31, Feb. 2001.
- [13] J. Wang and R. Rajamani, "Should adaptive cruise-control systems be designed to maintain a constant time gap between vehicles?" *IEEE Trans. Veh. Technol.*, vol. 53, no. 5, pp. 1480–1490, Sep. 2004.

- [14] J. Ploeg, N. van de Wouw, and H. Nijmeijer, “ L_p string stability of cascaded systems: Application to vehicle platooning,” *IEEE Trans. Control Syst. Technol.*, vol. 22, no. 2, pp. 786–793, Mar. 2014.
- [15] I. R. Wilmink, G. A. Klunder, and B. van Arem, “Traffic flow effects of Integrated Full-Range Speed Assistance (IRSA),” in *Proc. IEEE Intell. Veh. Symp.*, 2007, pp. 1204–1210.
- [16] D. Godbole, K. N. , R. Sengupta, and M. Zandonadi, “Breaking the highway capacity barrier: Adaptive cruise control-based concept,” *Transp. Res. Rec.*, vol. 1679, pp. 148–157, 1999.
- [17] K. Hasebe, A. Nakayama, and Y. Sugiyama, “Dynamical model of a cooperative driving system for freeway traffic,” *Phys. Rev. E*, vol. 68, no. 2, 2003, Art. ID 026102.
- [18] J. I. Ge and G. Orosz. “Dynamics of connected vehicle systems with delayed acceleration feedback,” *Transp. Res. C, Emerging Technol.*, vol. 46, pp. 46–64, Sep. 2014.
- [19] A. Kesting, M. Treiber, M. Schonhof, and D. Helbing, “Adaptive cruise control design for active congestion avoidance,” *Transp. Res. C, Emerging Technol.*, vol. 16, no. 6, pp. 668–683, Dec. 2008.
- [20] M. Treiber and A. Kesting, *Traffic Flow Dynamics—Data, Models and Simulation*. New York, NY, USA: Springer-Verlag, 2013.
- [21] J. A. Michon, *Generic Intelligent Driver Support*. New York, NY, USA: Taylor & Francis, 1993.
- [22] R. Miller and G. Nöcker, “Intelligent cruise control with fuzzy logic,” in *Proc. IEEE Intell. Veh. Symp.*, Detroit, MI, USA, 1992, pp. 173–178.
- [23] A. Shaout and M. Jarrah, “Cruise control technology review,” *Comput. Electr. Eng.*, vol. 23, no. 4, pp. 259–271, Jul. 1997.
- [24] K. Chu, “Decentralized control of high-speed vehicular strings,” *Transp. Sci.*, vol. 8, no. 4, pp. 361–384, Nov. 1974.
- [25] J. Mårtensson *et al.*, “The development of a cooperative heavy-duty vehicle for the GCDC 2011: Team scoop,” *IEEE Trans. Intell. Transp. Syst.*, vol. 13, no. 3, pp. 1033–1049, Sep. 2012.
- [26] S. Li, Z. Jia, K. Li, and B. Cheng, “Fast online computation of a model predictive controller and its application to fuel economy-oriented adaptive cruise control,” *IEEE Trans. Intell. Transp. Syst.*, vol. 16, no. 3, pp. 1199–1209, Jun. 2014.
- [27] M. Kamal, J. I. Imura, T. Hayakawa, A. Ohata, and K. Aihara, “Smart driving of a vehicle using model predictive control for improving traffic flow,” *IEEE Trans. Intell. Transp. Syst.*, vol. 15, no. 2, pp. 878–888, Apr. 2014.
- [28] S. P. Hoogendoorn, R. G. Hoogendoorn, M. Wang, and W. Daamen, “Modeling driver, driver support, and cooperative systems with dynamic optimal control,” *Transp. Res. Rec.*, vol. 2316, pp. 20–30, 2012.
- [29] M. Wang, “Generic model predictive control framework for advanced driver assistance systems,” Ph.D. dissertation, Dept. Transp. Plan., Delft Univ. Technol., Delft, The Netherlands, 2014.
- [30] W. B. Dunbar and R. M. Murray, “Distributed receding horizon control for multi-vehicle formation stabilization,” *Automatica*, vol. 42, no. 4, pp. 549–558, Apr. 2006.
- [31] R. Scattolini, “Architectures for distributed and hierarchical model predictive control—A review,” *J. Process Control*, vol. 19, no. 5, pp. 723–731, May 2009.
- [32] M. Wang, M. Treiber, W. Daamen, S. P. Hoogendoorn, and B. van Arem, “Modelling supported driving as an optimal control cycle: Framework and model characteristics,” *Transp. Res. C, Emerging Technol.*, vol. 36, pp. 547–563, 2013.
- [33] M. A. Müller, M. Reble, and F. Allgöwer, “Cooperative control of dynamically decoupled systems via distributed model predictive control,” *Int. J. Robust Nonlinear Control*, vol. 22, no. 12, pp. 1376–1397, Aug. 2012.
- [34] M. J. Lighthill and G. B. Whitham, “On kinematic waves II: A theory of traffic flow on long crowded roads,” *Proc. R. Soc. A*, vol. 229, no. 1178, pp. 317–345, May 1955.
- [35] M. J. Cassidy and R. L. Bertini, “Some traffic features at freeway bottlenecks,” *Transp. Res. B, Methodol.*, vol. 33, no. 1, pp. 25–42, Feb. 1999.
- [36] L. Leclercq, J. A. Laval, and N. Chiabaut, “Capacity drops at merges: An endogenous model,” *Transp. Res. B, Methodol.*, vol. 45, no. 9, pp. 1302–1313, 2011.
- [37] M. Treiber and A. Kesting, “Evidence of convective instability in congested traffic flow: A systematic empirical and theoretical investigation,” *Transp. Res. B, Methodol.*, vol. 45, no. 9, pp. 1362–1377, Nov. 2011.
- [38] C. M. J. Tampère, “Human-kinetic multiclass traffic flow theory and modelling—with application to advanced driver assistance systems in congestion,” Ph.D. dissertation, Dept. Technol. Eng., Delft Univ. Technol., Delft, The Netherlands, 2004.
- [39] J. A. Laval and C. F. Daganzo, “Lane-changing in traffic streams,” *Transp. Res. B, Methodol.*, vol. 40, no. 3, pp. 251–264, Mar. 2006.
- [40] M. Treiber, A. Kesting, and D. Helbing, “Understanding widely scattered traffic flows, the capacity drop, and platoons as effects of variance-driven time gaps,” *Phys. Rev. E*, vol. 74, pp. 10–16, 2006.
- [41] B. Coifman and S. Kim, “Extended bottlenecks, the fundamental relationship, and capacity drop on freeways,” *Transp. Res. A, Policy Pract.*, vol. 45, no. 9, pp. 980–991, Nov. 2011.
- [42] J. Treiterer and J. A. Myers, “The hysteresis phenomenon in traffic flow,” in *Proc. 6th Int. Symp. Transp. Traffic Theory*, 1974, pp. 13–38.
- [43] D. Chen, J. A. Laval, S. Ahn, and Z. Zheng, “Microscopic traffic hysteresis in traffic oscillations: A behavioral perspective,” *Transp. Res. B, Methodol.*, vol. 46, no. 10, pp. 1440–1453, Dec. 2012.
- [44] W. J. Schakel, V. Knoop, and B. van Arem, “Integrated lane change model with relaxation and synchronization,” *Transp. Res. Rec.*, vol. 2316, pp. 47–57, 2012.
- [45] R. Akcelik, “Efficiency and drag in the power-based model of fuel consumption,” *Transp. Res. B, Methodol.*, vol. 23, no. 5, pp. 376–385, Oct. 1989.
- [46] R. E. Wilson, “Mechanisms for spatio-temporal pattern formation in highway traffic models,” *Philosoph. Trans. R. Soc. A*, vol. 366, no. 1872, pp. 2017–2032, 2008.
- [47] M. Wang, S. P. Hoogendoorn, W. Daamen, B. van Arem and R. Happee, “Game theoretic approach for predictive lane-changing and car-following control,” *Transp. Res. C, Emerging Technol.*, vol. 58, pp. 73–92, Sep. 2015.



Meng Wang received the M.Sc. degree in transportation engineering from Research Institute of Highway, Beijing, China, in 2006 and the Ph.D. degree in transport and planning from Delft University of Technology, Delft, The Netherlands, in 2014. From 2014 to 2015, he was a Postdoctoral Researcher with the Department of BioMechanical Engineering, Delft University of Technology. Currently, he is an Assistant Professor with the Department of Transport and Planning, Delft University of Technology. His main research interests are driver behavior modeling and control approaches for intelligent vehicle systems.



Winnie Daamen received the M.Sc. and Ph.D. degrees in transport and planning from Delft University of Technology, Delft, The Netherlands, in 1998 and 2004, respectively. Currently, she is an Associate Professor with Delft University of Technology. She developed the pedestrian simulation model SimPed. Her current research involves modeling of drivers, ships, and pedestrians, as well as crowd management. To develop pedestrian models, she pioneered in pedestrian laboratory experiments and empirical observations on pedestrians. Her research interests also include empirical analysis of merging behavior on on-ramps.



Serge P. Hoogendoorn received the M.Sc. degree in applied mathematics and the Ph.D. degree in transport and planning from Delft University of Technology, Delft, The Netherlands, in 1995 and 1999, respectively. Currently, he is the Chair Professor of Traffic Flow Theory and Management with the Department of Transport and Planning, Delft University of Technology. His research involves theory, modeling, and simulation of traffic and transportation networks, focusing on innovative approaches to collect detailed microscopic traffic data and the use of these data to underpin the models and theories.



Bart van Arem (M'04) received the M.Sc. and Ph.D. degrees in applied mathematics from the University of Twente, Enschede, The Netherlands, in 1986 and 1990, respectively. From 1992 and 2009, he was a Researcher and a Program Manager with TNO, working on intelligent transport systems, in which he has been active in various national and international projects. Since 2009, he has been the Chair Professor of Transport Modeling with the Department of Transport and Planning, Delft University of Technology, Delft, The Netherlands, focusing on the impact of intelligent transport systems on mobility. His research interests include transport modelling and intelligent vehicle systems.